Available online at www.sciencedirect.com

SciVerse ScienceDirect

journal homepage: www.elsevier.com/locate/he

Synthesis of ammine dual-metal (V, Mg) borohydrides with enhanced dehydrogenation properties

Feng Yuan [a], Xiaowei Chen [a], Qinfen Gu [b], Ziwei Tang [a], Xuebin Yu [a,*]

[a] Department of Materials Science, Fudan University, 220 Handan Road, Shanghai 200433, China
[b] Australian Synchrotron, 800 Blackburn Rd, Clayton 3168, Australia

ARTICLE INFO

Article history:
Received 22 October 2012
Received in revised form
7 February 2013
Accepted 9 February 2013
Available online 19 March 2013

Keywords:
Hydrogen storage
Ammine metal borohydrides
Metathesis reaction
Dehydrogenation mechanism

ABSTRACT

The penta-ammine vanadium (III) borohydride, i.e. $V(BH_4)_3 \cdot 5NH_3$, was successfully synthesized via ball-milling of $VCl_3 \cdot 5NH_3$ and $LiBH_4$ in a molar ratio of 1:3. This compound was shown to release 11.5 wt% hydrogen with a H_2-purity of 85 mol% by 350 °C. To improve the dehydrogenation purity of $V(BH_4)_3 \cdot 5NH_3$, $Mg(BH_4)_2$ with various molar ratios was mixed with $V(BH_4)_3 \cdot 5NH_3$ to synthesize expected ammine metal-mixed borohydrides, among which the formed $VMg(BH_4)_5 \cdot 5NH_3$ was indexed to be a monoclinic unit cell with lattice parameters of $a = 19.611$ Å, $b = 14.468$ Å, $c = 6.261$ Å, $\beta = 93.678°$ and $V = 1772.75$ Å^3. Dehydrogenation results revealed that the $Mg(BH_4)_2$ modified $V(BH_4)_3 \cdot 5NH_3$ system presents significantly enhanced dehydrogenation purity. For example, in the case of $V(BH_4)_3 \cdot 5NH_3/2Mg(BH_4)_2$ sample, 12.4 wt% pure hydrogen can be released upon heating to 300 °C. Further investigation on the dehydrogenation mechanism of the $VMg(BH_4)_5 \cdot 5NH_3$ system by isotope tagging revealed that the interactions of homo-polar BH units also participated throughout the dehydrogenation process (onset at 75 °C) as complementary to the prime combination of BH···HN.

1. Introduction

The development and use of hydrogen, which is abundant and eco-friendly, is regarding as an efficient strategy for solving the energy and environment concerns [1,2]. The achievement of safe, economic, compact and high efficient density hydrogen storage is one of the key challenges in the implementation of hydrogen-based energy society [3,4]. Among all the discovered hydrogen storage systems, including classical high-pressure tanks, hydrogen adsorption on solid surfaces and etc., chemical complexes, such as alanates [5], amides [6] and borohydrides [7], show an important advantage with respect to their high hydrogen gravimetric density. However, the practical use of these hydrides as hydrogen storage materials is obstructed either by their high dehydrogenation temperature because of both kinetic and thermodynamic limitations [8–10], or by accompanying release of impurities (e.g. NH_3, B_2H_6 and etc.) [6,11], or even by the instability of hydrides themselves at ambient temperature [12–15].

Recently, researches have demonstrated that the hydrogen-enriched BNH system, of which the hydrogen release is mainly based on the combination of BH and NH units, is an alternative and promising strategy to develop new substances which can release hydrogen at practical temperature and pressure [16–24]. Among these reported BNH system [25–27], the ammine metal borohydrides (AMBs) system has been demonstrated to be one of the most promising hydrogen storage systems due to their high gravimetric hydrogen density and favorable dehydrogenation

* *Corresponding author*. Tel./fax: +86 21 5566 4581.
E-mail address: yuxuebin@fudan.edu.cn (X. Yu).

0360-3199/$ – see front matter
http://dx.doi.org/10.1016/j.ijhydene.2013.02.039

kinetics and thermodynamics [28–32]. Recently, we developed a new technique [33–35], i.e. metathesis reaction between metal chloride ammoniates and lithium or sodium borohydride by mechanical milling, to synthesize various AMBs, which provides a general solution to develop novel AMBs that cannot be obtained by the traditional access.

Although AMBs exhibited satisfied dehydrogenation kinetics and thermodynamics, the release of ammonia byproduct upon decomposition is a common shortcoming suffered by most of AMBs [28–32,36]. Previous researches have revealed that the dehydrogenation purity of AMBs relies on both the Pauling electronegativity (χ_p) of central metal and the balance of BH and NH units, i.e., higher χ_p and balanced BH/NH ratio contribute to the higher dehydrogenation purity [33,37,38]. More recently, significant dehydrogenation improvements were achieved for $Al(BH_4)_3\cdot 6NH_3$ and $Ca(BH_4)_2\cdot NH_3$ via combining with $LiBH_4$ to promote the BH···NH reaction [39,40], indicating that the introduction of mixed metal is an another effective strategy for improving the dehydrogenation properties of AMBs [39,41,42].

$$VCl_3\cdot 5NH_3 + 3LiBH_4 \rightarrow V(BH_4)_3\cdot 5NH_3 + 3LiCl \quad (1)$$

$$V(BH_4)_3\cdot 5NH_3 + Mg(BH_4)_2 \rightarrow VMg(BH_4)_5\cdot 5NH_3 \quad (2)$$

In this paper, $V(BH_4)_3\cdot 5NH_3$ was firstly synthesized according to the metathesis reaction of Eq. (1). And then, guided by the previously reported metal-aided strategy, $Mg(BH_4)_2$ was ball-milled with the synthesized $V(BH_4)_3\cdot 5NH_3$ to form V–Mg-based ammine metal-mixed borohydride, according to Eq. (2), which is expected to optimize the dehydrogenation properties of plain $V(BH_4)_3\cdot 5NH_3$. Dehydrogenation results revealed that the combined ammine metal-mixed borohydrides are able to release over 10% pure hydrogen without any undesirable byproducts, demonstrating their potential for hydrogen storage application. Furthermore, isotope tagging mass spectrometer discovered that the interactions of homo-polar BH units actually participated in the dehydrogenation process of the $Mg(BH_4)_2$-modified $V(BH_4)_3\cdot 5NH_3$ system as a supplementary dehydrogenation pathway.

2. Experimental section

2.1. Synthesis

Anhydrous starting materials ($LiBH_4$, 95%; $NaBH_4$, 97%; $NaBD_4$, 95%; $NaAlH_4$, 98%; VCl_3, 97%; $MgCl_2$, 99%) were purchased from Sigma–Aldrich and used directly without further purification, while NH_3 (Alfa Aesar) was purified by soda lime before using, and anhydrous diethyl ether (Sigma–Aldrich) was further dried using $NaAlH_4$. All solid samples were handled in a glovebox equipped with a recirculation and regeneration system, which maintain the oxygen and water concentrations below 1 ppm.

$$VCl_3 + 5NH_3 \rightarrow VCl_3\cdot 5NH_3\cdot \quad (3)$$

$VCl_3\cdot 5NH_3$ was firstly prepared by exposing VCl_3 to NH_3 atmosphere according to Eq. (3). Approximately 0.5 g (typical weight) VCl_3 was transferred to the reaction vessel under argon atmosphere. After the argon was evacuated, the purified ammonia was purged and kept for 3 h until the VCl_3 sample was saturated. After the excessive ammonia was evacuated, the molar ratio of NH_3 to VCl_3 for the saturated salt was determined gravimetrically to be 4.97, confirming the formation of $VCl_3\cdot 5NH_3$. The TPD result of $VCl_3\cdot 5NH_3$ is shown in Figure S1.

$Mg(BH_4)_2$ ($Mg(BD_4)_2$) was synthesized from $NaBH_4$ ($NaBD_4$) and $MgCl_2$ in anhydrous diethyl ether based on the description in previous report [43].

Ammine vanadium borohydrides were prepared by ball-milling mixtures of $VCl_3\cdot 5NH_3$–$LiBH_4$ (in a molar ratio of 1:3) using planetary QM-3SP2 with a ball-to-sample ratio of 30:1, agitation frequency of 350 rpm. Nominal V–Mg-based ammine dual-metal borohydrides were prepared by ball-milling mixtures of $V(BH_4)_3\cdot 5NH_3$(3LiCl)/$Mg(BH_4)_2$ (1:1 and 1:2) using planetary QM-3SP2 with agitation frequency of 280 rpm. To avoid an increasing temperature of the powders in the vessel, the milling process was carried out alternating 6 min of milling and 6 min of stop.

2.2. Instrument and analysis

Temperature-programmed-desorption (TPD) measurement was carried out on a semi-automatic Sievert's apparatus under argon atmosphere (~1 bar) with a heating rate of 5 °C/min.

The dehydrogenation properties of the as-prepared samples were examined by simultaneous thermal gravimetric analysis (TGA) combined with a mass spectrometer (MS, QMS 403) in which about 6 mg samples were heated at a heating rate of 5 °C/min ranging from room temperature to 300 °C under argon flow. Differential scanning calorimetry (DSC) was performed by TAQ 2000 DSC under argon with a gas flow of 50 mL Ar min^{-1} at a heating rate of 5 °C/min. All weight loss presented in this article is calculated with LiCl being viewed as an inert bystander.

For phase identification and structure determination, the sample was loaded into a pre-dried 0.7 mm boron–silica glass capillary whilst inside an argon-filled glovebox. Synchrotron powder X-ray diffraction data were collected by a Mythen-II detector with the wavelength 0.9528 Å at the Powder diffraction beamline, Australian Synchrotron. The capillary was sealed with vacuum grease for X-ray diffraction measurements. In order to identify the reaction products and estimate the crystallinity of the sample, time-resolved *in-situ* measurements were conducted by using a Cyberstar hot-air blower to heat the sample from 30 °C to 170 °C at a constant heating rate of 6 °C/min. Data were collected with an exposure time of 150 s at every 10 °C step.

Fourier transform infrared (FTIR) (Magna-IR 550 II, Nicolet) analyses were conducted to confirm the chemical bonds in all solid products. Products were pressed with KBr and then loaded into a sealed chamber with CaF_2 window for the measurement. Anhydrous KBr was used as a pellet material.

3. Results and discussion

The $V(BH_4)_3\cdot 5NH_3$ was synthesized via the mechanochemical solid/solid reaction as described in Eq. (1). The products of this

reaction were verified by high-resolution XRD and FTIR. As shown in Fig. 1c, the diffraction peaks of the ball-milled $VCl_3{\cdot}5NH_3$–$3LiBH_4$ consist of LiCl and some unassignable peaks, and the starting materials $LiBH_4$ and $VCl_3{\cdot}5NH_3$ totally disappeared, suggesting that the metathesis reaction proceeded successfully, resulting in the formation of $V(BH_4)_3{\cdot}5NH_3$ and LiCl. Moreover, no apparent pressure fluctuation was detected during the ball-milling, indicating that the NH_3 groups entirely remained during the metathesis reaction to form $V(BH_4)_3{\cdot}5NH_3$. It should be noted that there is no crystal information for $VCl_3{\cdot}5NH_3$ and $V(BH_4)_3{\cdot}5NH_3$ in the ICDD, ICSD and CSD databases. However, our endeavors to solve the structures of these two compounds failed due to their poor crystallinity. By further ball-milling $V(BH_4)_3{\cdot}5NH_3$ and $Mg(BH_4)_2$ with a molar ratio of 1:1, $VMg(BH_4)_5{\cdot}5NH_3$ was obtained according to Eq. (2). Bragg peaks in the room temperature diffraction pattern from $VMg(BH_4)_5{\cdot}5NH_3$ were indexed to be a monoclinic unit cell with lattice parameters of a = 19.611 Å, b = 14.468 Å, c = 6.261 Å, β = 93.678° and V = 1772.75 Å^3 using code DICVOL06 [44]. Further analysis of systematic extinction, the suggesting space group is $P2/m$ or $P2_1/m$. Unfortunately, our endeavors to locate the accurate atomic positions with direct space method also failed due to its structure complexity.

By the combination of TPD results conducted by volumetric measurement in a close system (Fig. 2) and gravimetric results of residual solids, ca. 11.5 wt% hydrogen, accompanied with a certain amount of ammonia (ca. 17.1 wt%), were released from $V(BH_4)_3{\cdot}5NH_3$ upon heating to 250 °C. To optimize the dehydrogenation properties of $V(BH_4)_3{\cdot}5NH_3$, 6 mol LiH were added to this compound to equal the quantity of $H^{\delta+}$ in redundant NH_3 relative to BH_4 groups. Moreover, to obtain ammine metal-mixed borohydrides, $LiBH_4$ and $Mg(BH_4)_2$ were also milled with $V(BH_4)_3{\cdot}5NH_3$, respectively. The TPD results of $V(BH_4)_3{\cdot}5NH_3$ + 6LiH, $V(BH_4)_3{\cdot}5NH_3$ + $2LiBH_4$ and $VMg(BH_4)_5{\cdot}5NH_3$ are shown in Fig. 2. A summary of the gravimetric and volumetric results for $V(BH_4)_3{\cdot}5NH_3$ and $V(BH_4)_3{\cdot}5NH_3$/additives are listed in Table 1. It can be seen that the hydrogen purity is increased from 85 mol % for $V(BH_4)_3{\cdot}5NH_3$ to 89 mol%, 90.7 mol%, 96 mol% and 100 mol % for $V(BH_4)_3{\cdot}5NH_3$ + 6LiH, $V(BH_4)_3{\cdot}5NH_3$ + $2LiBH_4$, $VMg(BH_4)_5{\cdot}5NH_3$ and $V(BH_4)_3{\cdot}5NH_3$ + $2Mg(BH_4)_2$ respectively. Clearly, addition of $Mg(BH_4)_5$ presents the best results on enhancing the dehydrogenation purity of $V(BH_4)_3{\cdot}5NH_3$.

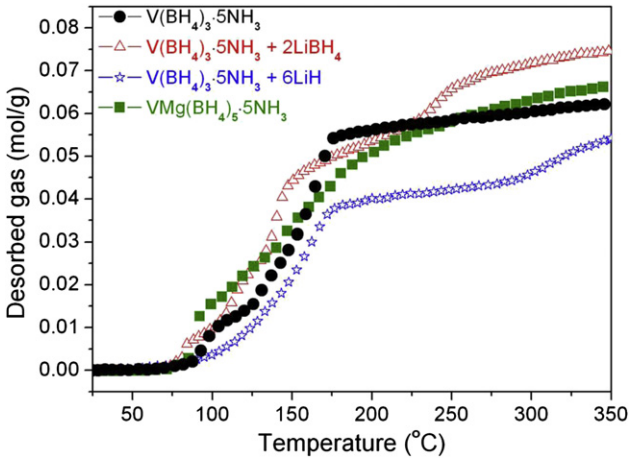

Fig. 2 – TPD results of $V(BH_4)_3{\cdot}5NH_3$ (filled dots), $V(BH_4)_3{\cdot}5NH_3$ + $2LiBH_4$ (open triangles), $V(BH_4)_3{\cdot}5NH_3$ + 6LiH (open stars) and $VMg(BH_4)_5{\cdot}5NH_3$ (filled rectangles). These volumetric contents are calculated with LiCl being viewed as dead mass.

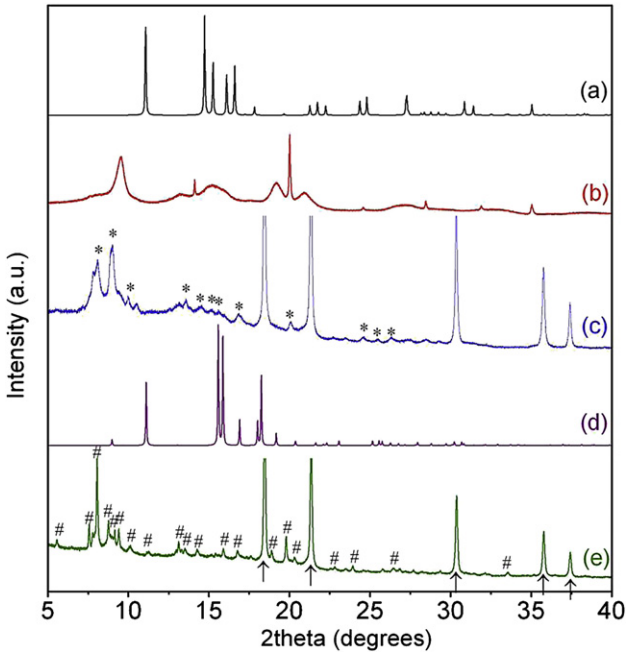

Fig. 1 – High-resolution XRD results of (a) $LiBH_4$, (b) $VCl_3{\cdot}5NH_3$, (c) milled $VCl_3{\cdot}5NH_3$–$LiBH_4$ (molar ratio of 1:3), (d) $Mg(BH_4)_2$ and (e) milled $V(BH_4)_3{\cdot}5NH_3$ + $Mg(BH_4)_2$. LiCl (↑), $V(BH_4)_3{\cdot}5NH_3$ (*) and $VMg(BH_4)_5{\cdot}5NH_3$ (#).

A comparison of TG–DSC–MS traces for $V(BH_4)_3{\cdot}5NH_3$ and $Mg(BH_4)_2$-modified $V(BH_4)_3{\cdot}5NH_3$ recorded under ramping temperature conditions is presented in Fig. 3. For $V(BH_4)_3{\cdot}5NH_3$, a two-step decomposition in the temperature range of 80–250 °C, with a total weight loss of 35.8 wt%, was observed. The first section occurred in the temperature range of 80–110 °C, in which two main hydrogen evolution peaks located at 100 and 105 °C, without releasing of any impurities (i.e. NH_3 and B_2H_6). The DSC profile in this temperature region shows an exothermic reaction which fits well with the hydrogen evolution. The second decomposition step occurred in 110–250 °C with vigorous hydrogen release peaked at 138 and 155 °C, which nevertheless accompanied with a fraction of ammonia emission, resulting in an endothermic phenomenon as observed in the DSC plot.

While after the introduction of one mole $Mg(BH_4)_2$ to this system, the decomposition pathway changed to four steps in the temperature range of 65–280 °C with four explicit peaks located at 78, 108, 134 and 247 °C, respectively. TG results gave a total mass loss of 23.1 wt%, which is 12.7 wt% less than that of $V(BH_4)_3{\cdot}5NH_3$, suggesting the effective suppression of ammonia emission, in which, except for a slight evolution of ammonia in the third stage, the other three stages were dominated by pure hydrogen release. DSC profile of $VMg(BH_4)_5{\cdot}5NH_3$ shows significant differences compared with

Table 1 – The summary of gas evolution and reaction enthalpy from $V(BH_4)_3 \cdot 5NH_3$ and its composites.

Samples[a]	wt% H_2 capacity	wt% NH_3 capacity	mol% H_2[b]	ΔH (kJ/mol)[c]		
				1st	2nd	3rd
$V(BH_4)_3 \cdot 5NH_3$	11.5	17.1	85	−33.5	48	/
$V(BH_4)_3 \cdot 5NH_3 + 6LiH$	10.3	10.7	89			
$V(BH_4)_3 \cdot 5NH_3 + 2LiBH_4$	13.5	11.7	90.7			
$VMg(BH_4)_5 \cdot 5NH_3$	12.7	4.5	96	−37.6	/	4.8
$V(BH_4)_3 \cdot 5NH_3 + 2Mg(BH_4)_2$	12.4	0	100	/	/	/

a The samples were heated under 1 bar argon atmosphere from RT to 400 °C with a heating rate of 5 °C/min by TPD in a close system.
b H_2 molar ratio in the released gas.
c Curve-fitting of the DSC trace gave an approximate value for the reaction enthalpy.

that of $V(BH_4)_3 \cdot 5NH_3$. A sharp exothermic effect at 80 °C was observed, which corresponds to the intensive exothermic effect derived from the combination of BH and NH units. Meanwhile, the mild endothermic peak around 155 °C could be associated with the slight ammonia emission occurred in the third decomposition stage.

With further increasing the ratio of $Mg(BH_4)_2$ to two moles, the onset decomposition temperature decreased to 55 °C, which is 10 °C and 25 °C lower than that of $VMg(BH_4)_5 \cdot 5NH_3$ and $V(BH_4)_3 \cdot 5NH_3$, respectively. The $V(BH_4)_3 \cdot 5NH_3 + 2Mg(BH_4)_2$ sample was shown to release pure hydrogen via four steps with peaks at 73, 100, 180 and 224 °C, respectively. No emission of borazine and/or ammonia was detected (Fig. 3c). TG result shows that about 12.4 wt% pure hydrogen is released throughout the thermal decomposition process. Three mild exothermic peaks at 66, 96 and 178 °C, corresponding to the former three stages, can be observed in DSC profile, suggesting the similar hydrogen desorption mechanism with that of $VMg(BH_4)_5 \cdot 5NH_3$, while the additional endothermic peak at 223 °C could be ascribed to the decomposition of surplus BH_4^- groups in the fourth step.

As indicated by the MS results above, the ammonia release in the $VMg(BH_4)_5 \cdot 5NH_3$ is only occurring in the third step. To obtain the dehydrogenation properties of $VMg(BH_4)_5 \cdot 5NH_3$ at different temperatures region, the isothermal desorption kinetics measurement was conducted and the results are shown in Fig. 4. It shows that the hydrogen release starts immediately without any induction period. At 160 °C, the hydrogen release is completed within 50 min with a capacity of 9.9 wt% H_2. For the sample held at 100 °C, 120 °C and 150 °C, about 7.9 wt%, 8.2 wt% and 9.7 wt% H_2 are generated within 500 min, respectively. Interestingly, on the contrary to the tendency that the hydrogen release contents increased with the increased

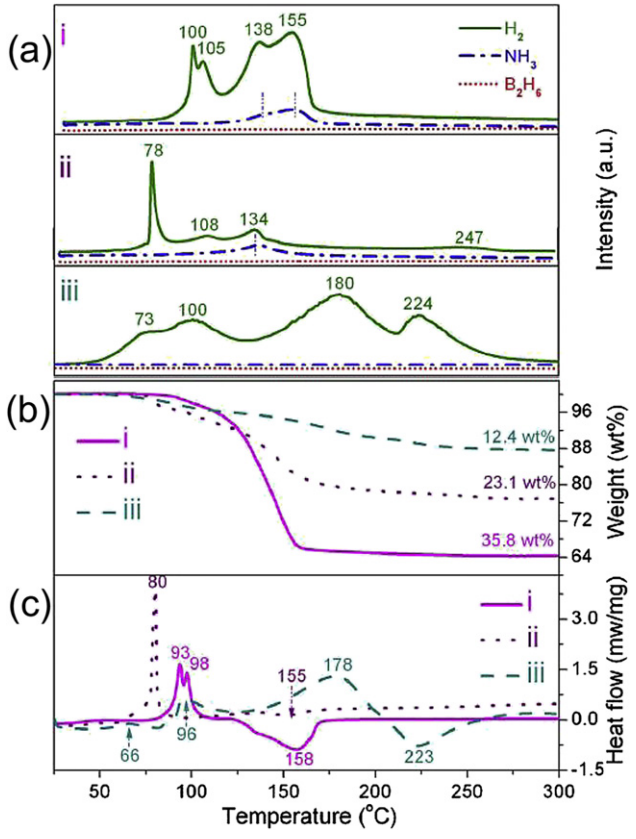

Fig. 3 – (a) MS, (b) TG and (c) DSC profiles of (i) $V(BH_4)_3 \cdot 5NH_3$, (ii) $VMg(BH_4)_5 \cdot 5NH_3$ and (iii) $V(BH_4)_3 \cdot 5NH_3/2Mg(BH_4)_2$ respectively. The content of desorbed gas is calculated accounting for the weights of pure $V(BH_4)_3 \cdot 5NH_3$, $VMg(BH_4)_5 \cdot 5NH_3$ and $V(BH_4)_3 \cdot 5NH_3/2Mg(BH_4)_2$, respectively.

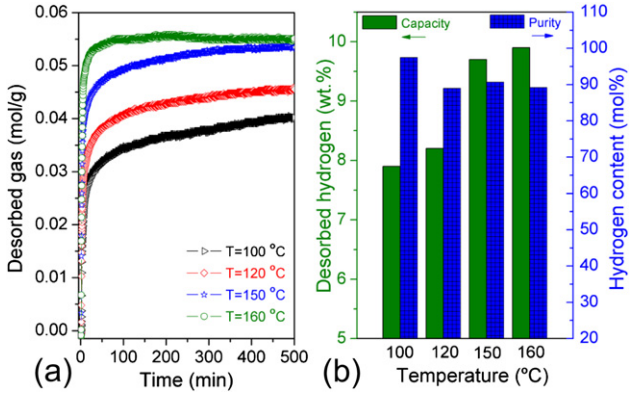

Fig. 4 – (a) Isothermal TPD results for $VMg(BH_4)_5 \cdot 5NH_3$. Pattern (b) is the summary of hydrogen and ammonia release at different temperature. These volumetric and gravimetric capacities are calculated relative to the $VMg(BH_4)_5 \cdot 5NH_3$ weight only.

temperatures, the hydrogen purity decreased along with the elevated temperatures except for a slight fluctuate at 120 °C.

High-resolution *in-situ* XRD measurement was conducted for $V(BH_4)_3 \cdot 5NH_3$ and $VMg(BH_4)_5 \cdot 5NH_3$ samples to further depict their thermal decomposition processes. As shown in Fig. 5a, a slightly enhanced crystallinity is observed for $V(BH_4)_3 \cdot 5NH_3$ upon heating to 90 °C, confirmed by the fact that the peaks from $V(BH_4)_3 \cdot 5NH_3$ became narrower and the peaks intensity increased. With further increasing the temperature, $V(BH_4)_3 \cdot 5NH_3$ starts to decompose and totally transforms into amorphous at 150 °C. As for $VMg(BH_4)_5 \cdot 5NH_3$ (Fig. 5b), the diffraction peaks keep unchanged until 80 °C, and then the peaks intensity starts to decrease upon further heating to

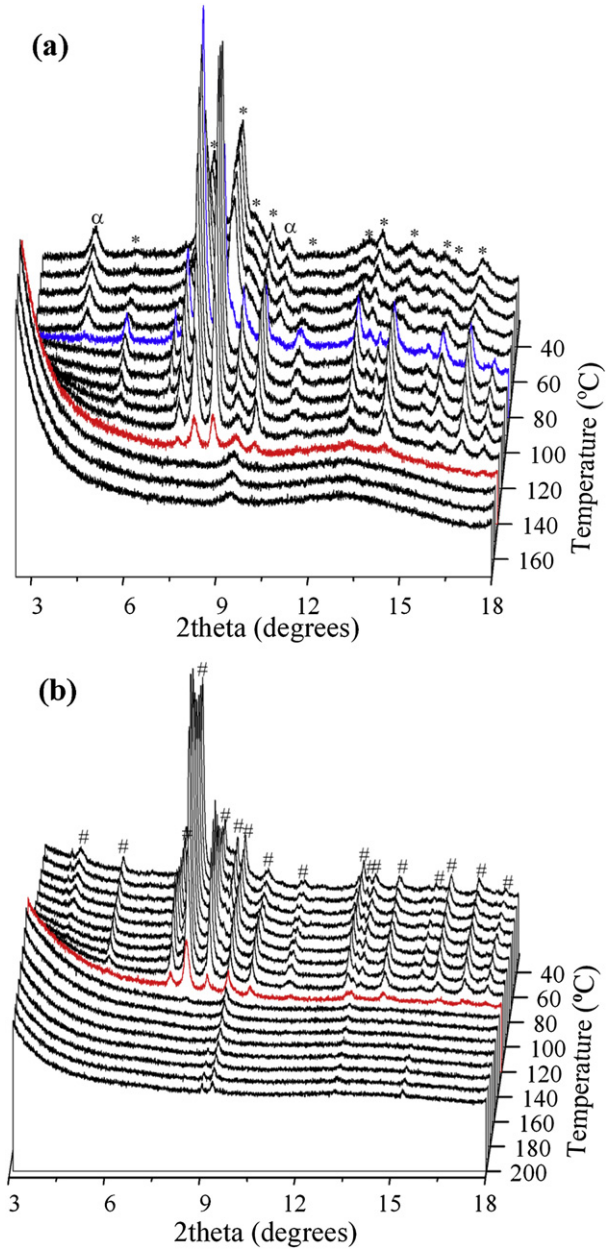

Fig. 5 – Selected *in-situ* high-resolution XRD patterns for (a) $V(BH_4)_3 \cdot 5NH_3$ and (b) $VMg(BH_4)_5 \cdot 5NH_3$ composites. Impurity (α), $V(BH_4)_3 \cdot 5NH_3$ (*) and $VMg(BH_4)_5 \cdot 5NH_3$ (#).

higher temperature, and eventually vanishes at 130 °C, suggesting the decomposition of $VMg(BH_4)_5 \cdot 5NH_3$ accompanied with the emission of hydrogen, which is in good accordance with the observation of TG–MS measurements. In addition, peaks of LiCl in these two compounds (not given here) keep unchanged throughout the heating process, indicating that LiCl indeed acted as an inert bystander.

The IR spectra of $V(BH_4)_3 \cdot 5NH_3$ and $VMg(BH_4)_5 \cdot 5NH_3$ measured at different temperatures are presented in Fig. 6. As shown in Fig. 6a, the $V(BH_4)_3 \cdot 5NH_3$ at room temperature shows bands at equivalent numbers: i.e., (i) effected by OH stretching bands but distinguishable small absorption bands in the NH stretching region (3031–3266 cm^{-1}); (ii) three strong BH stretching adsorption bands located at 2223, 2292 and 2384 cm^{-1}, respectively, which are similar to that of borohydrides, indicating the entire transformation of BH_4 units from $LiBH_4$ to $V(BH_4)_3 \cdot 5NH_3$; (iii) intensive NH bending adsorption peak at 1403 cm^{-1}; (iv) one intense BH bending adsorption peak, along with other weaker two, at 1122, 1185 and 1254 cm^{-1}, respectively. Upon heating to 130 °C, the peaks assigned to both BH and NH vibrations are all diminished, along with the appearance of BN stretching region (864–1025 cm^{-1}) [45], suggesting the consume of BH and NH in $V(BH_4)_3 \cdot 5NH_3$ and the formation of BN-like residue during dehydrogenation [33,41]. On further heating to 300 °C, after which the dehydrogenation reaction is accomplished, vibrations associated with BH units disappear, while vibrations assigned to NH groups are still remained, suggesting the excessive supplement of NH during the decomposition, which is in consistent with the unbalanced numbers of NH_3 and BH_4 groups in $V(BH_4)_3 \cdot 5NH_3$. At the same time, the intensity of the BN stretching bands is increased, indicating that the final solid residue is BN-like amorphous compound. In addition, $VMg(BH_4)_5 \cdot 5NH_3$ (Fig. 6b) possesses the analogous FTIR characters as $V(BH_4)_3 \cdot 5NH_3$, i.e. the vanishment of BH and NH groups and the formation of BN-like amorphous product upon heating.

Previous works have established that the NH···HB proton-hydride (dihydrogen) interactions play an important role in the stability of the solid-state architecture and further in the evolution of hydrogen in the BN-based hydride system [16,46], and, in general, the participation of the homo-polar BH···HB pathway in low temperature is counterintuitive given the homo-polar nature of these two BH units involved. However, in a recent work, the BH···HB interaction was observed by isotope tagging [47,48]. In order to glean further clues for the thermal decomposition mechanism, we ball-milled $V(BH_4)_3 \cdot 5NH_3$ with $Mg(BD_4)_2$ to form '$VMg(BH_4)_3(BD_4)_2 \cdot 5NH_3$', and investigated this sample by MS measurement to identify the provenances of H_2, HD and D_2. As shown in Fig. 7, the liberation of H_2, HD and D_2 presents the similar trend in spite of different capacity levels. The onset of D_2 evolution, which derived from the interactions of homo-polar BD units, occurs at 75 °C, just slightly higher than that of H_2, suggesting that the contribution to hydrogen formation from the interactions of homo-polar BH units is always occurring as complementary to the NH···HB interactions throughout the thermal decomposition process. Therefore from another point of view, to completely suppress the NH_3 emission in $V(BH_4)_3 \cdot 5NH_3$ system, the number of BH_4 groups should be increased to be more

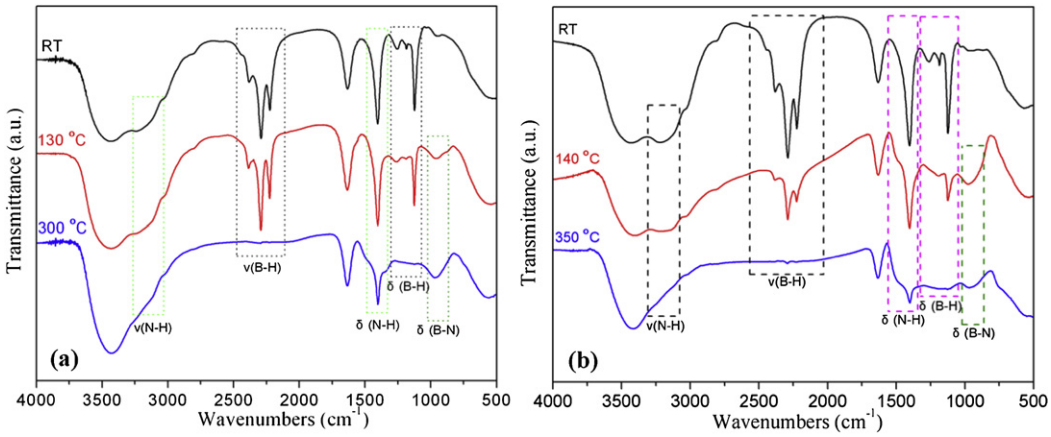

Fig. 6 – FTIR spectra of (a) $V(BH_4)_3 \cdot 5NH_3$ and (b) $VMg(BH_4)_5 \cdot 5NH_3$ after heating to various temperatures.

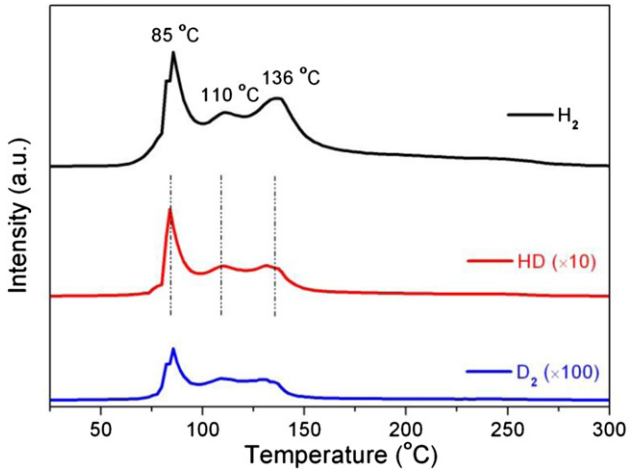

Fig. 7 – MS pattern of as-prepared $V(BH_4)_3 \cdot 5NH_3/Mg(BD_4)_2$ sample with a heating rate of 5 °C/min.

than that of NH_3 groups because the accompanied BH units interaction will consume the BH_4 groups and thus decrease the NH···HB interaction. This was confirmed by the pure hydrogen release from the $V(BH_4)_3 \cdot 5NH_3/2Mg(BH_4)_2$.

4. Conclusions

The penta-ammine vanadium (III) borohydride, i.e. $V(BH_4)_3 \cdot 5NH_3$, has been successfully synthesized via the metathesis reaction between vanadium trichloride penta-ammoniates and lithium borohydride. Following that, guided by the previously reported metal-aided strategy, $Mg(BH_4)_2$ was ball-milled with $V(BH_4)_3 \cdot 5NH_3$ to form ammine metal-mixed borohydrides. The higher hydrogen release content, enhanced hydrogen emission purity and lower decomposition temperature enable the $Mg(BH_4)_2$-modified $V(BH_4)_3 \cdot 5NH_3$ to be potential candidates as hydrogen storage materials. In addition, by using isotope tagging, it was observed that the interactions of homo-polar BH units in $VMg(BH_4)_5 \cdot 5NH_3$ actually occurred during the dehydrogenation process, which sheds light on the hydrogen release mechanism, especially on the realization of complete suppression of NH_3 emission in this kind of hydrogen storage materials.

Acknowledgement

This work was partially supported by the Ministry of Science and Technology of China (2010CB631302), the National Natural Science Foundation of China (51071047, 21271046), the PhD Programs Foundation of Ministry of Education of China (20110071110009) and Science and Technology Commission of Shanghai Municipality (11JC1400700, 11520701100).

Appendix A. Supplementary data

Supplementary data related to this article can be found at http://dx.doi.org/10.1016/j.ijhydene.2013.02.039.

REFERENCES

[1] Dresselhaus M, Thomas I. Alternative energy technologies. Nature 2001;21:19–29.
[2] Eberle U, Felderhoff M, Schüth F. Chemical and physical solutions for hydrogen storage. Angewandte Chemie International Edition 2009;48:6608–30.
[3] Schlapbach L, Züttel A. Hydrogen-storage materials for mobile applications. Nature 2001;414:353–8.
[4] Yang J, Sudik A, Wolverton C, Siegel DJ. High capacity hydrogen storage materials: attributes for automotive applications and techniques for materials discovery. Chemical Society Reviews 2010;39:656–75.
[5] Bogdanovic B, Schwickardi M. Ti-doped alkali metal aluminium hydrides as potential novel reversible hydrogen storage materials. Journal of Alloys and Compounds 1997;253:1–9.

[6] Chen P, Xiong Z, Luo J, Lin J, Tan KL. Interaction of hydrogen with metal nitrides and imides. Nature 2002;420:302–4.
[7] Orimo S, Nakamori Y, Eliseo JR, Züttel A, Jensen CM. Complex hydrides for hydrogen storage. Chemical Reviews 2007;107:4111–32.
[8] Züttel A, Rentsch S, Fischer P, Wenger P, Sudan P, Mauron P, et al. Hydrogen storage properties of $LiBH_4$. Journal of Alloys and Compounds 2003;356:515–20.
[9] Chłopek K, Frommen C, Léon A, Zabara O, Fichtner M. Synthesis and properties of magnesium tetrahydroborate, $Mg(BH_4)_2$. Journal of Materials Chemistry 2007;17:3496–503.
[10] Mao JF, Guo ZP, Nevirkovets IP, Liu HK, Dou SX. Hydrogen de-/absorption improvement of $NaBH_4$ catalyzed by titanium-based additives. Journal of Physical Chemistry C 2012;116:1596–604.
[11] Nakamori Y, Miwa K, Ninomiya A, Li H, Ohba N, Towata S, et al. Correlation between thermodynamical stabilities of metal borohydrides and cation electronegativities: first-principles calculations and experiments. Physical Review B 2006;74:045126.
[12] Weidenthaler C, Pommerin A, Felderhoff M, Sun W, Wolverton C, Bogdanović B, et al. Complex rare-earth aluminum hydrides: mechanochemical Preparation, crystal structure and potential for hydrogen storage. Journal of the American Chemical Society 2009;131:16735–43.
[13] Guo YH, Yu XB, Gao L, Xia GL, Guo ZP, Liu HK. Significantly improved dehydrogenation of $LiBH_4$ destabilized by TiF_3. Energy & Environmental Science 2009;3:465–70.
[14] Marks TJ, Kolb JR. Covalent transition metal, lanthanide, and actinide tetrahydroborate complexes. Chemical Reviews 1977;77:263–93.
[15] Yang CH, Tsai WT, Chang JK. Hydrogen desorption behavior of vanadium borohydride synthesized by modified mechano-chemical process. International Journal of Hydrogen Energy 2012.
[16] Staubitz A, Robertson APM, Manners I. Ammonia–borane and related compounds as dihydrogen sources. Chemical Reviews 2010;110:4079–124.
[17] Xiong ZT, Yong CK, Wu GT, Chen P, Shaw W, Karkamkar A, et al. High-capacity hydrogen storage in lithium and sodium amidoboranes. Nature Materials 2007;7:138–41.
[18] Wu CZ, Wu GT, Xiong ZT, Han XW, Chu HL, He T, et al. $LiNH_2BH_3{\bullet}NH_3BH_3$: structure and hydrogen storage properties. Chemistry of Materials 2010;22:3–5.
[19] Xia GL, Yu XB, Guo YH, Wu Z, Yang CZ, Liu HK, et al. Amminelithium amidoborane $Li(NH_3)NH_2BH_3$: a new coordination compound with favorable dehydrogenation characteristics. Chemistry-A European Journal 2010;16:3763–9.
[20] Sudik A, Yang J, Halliday D, Wolverton C. Hydrogen storage properties in $(LiNH_2)_2$–$LiBH_4$–$(MgH_2)_X$ mixtures ($X = 0.0$–1.0). Journal of Physical Chemistry C 2008;112:4384–90.
[21] Matsuo M, Remhof A, Martelli P, Caputo R, Ernst M, Miura Y, et al. Complex hydrides with $(BH_4)^-$ and $(NH_2)^-$ anions as new lithium fast-ion conductors. Journal of the American Chemical Society 2009;131:16389–91.
[22] Gao L, Guo YH, Xia GL, Yu XB. Low temperature hydrogen generation from ammonia combined with lithium borohydride. Journal of Materials Chemistry 2009;19:7826–9.
[23] Tan YB, Guo YH, Li SF, Sun WW, Zhu YH, Li Q, et al. A liquid-based eutectic system: $LiBH_4{\cdot}NH_3$–$n NH_3BH_3$ with high dehydrogenation capacity at moderate temperature. Journal of Materials Chemistry 2011;21:14509–15.
[24] Tang ZW, Chen H, Chen XW, Wu LM, Yu XB. Graphene oxide based recyclable dehydrogenation of ammonia borane within a hybrid nanostructure. Journal of the American Chemical Society 2012;134:5464–7.
[25] Hamilton CW, Baker RT, Staubitz A, Manners I. B–N compounds for chemical hydrogen storage. Chemical Society Reviews 2009;38:279–93.
[26] Sudik A, Yang J, Siegel DJ, Wolverton C, Carter RO, Drews AR. Impact of stoichiometry on the hydrogen storage properties of $LiNH_2$–$LiBH_4$–MgH_2 ternary composites. Journal of Physical Chemistry C 2009;113:2004–13.
[27] Staubitz A, Sloan ME, Robertson APM, Friedrich A, Schneider S, Gates PJ, et al. Catalytic dehydrocoupling/dehydrogenation of *N*-methylamine-borane and ammonia–borane: synthesis and characterization of high molecular weight polyaminoboranes. Journal of the American Chemical Society 2010;132:13332–45.
[28] Soloveichik G, Her JH, Stephens PW, Gao Y, Rijssenbeek J, Andrus M, et al. Ammine magnesium borohydride complex as a new material for hydrogen storage: structure and properties of $Mg(BH_4)_2{\bullet}2NH_3$. Inorganic Chemistry 2008;47:4290–8.
[29] Johnson SR, David WIF, Royse DM, Sommariva M, Tang CY, Fabbiani F, et al. The monoammoniate of lithium borohydride, $Li(NH_3)BH_4$: an effective ammonia storage compound. Chemistry-An Asian Journal 2009;4:849–54.
[30] Chu HL, Wu GT, Xiong ZT, Guo JP, He T, Chen P. Structure and hydrogen storage properties of calcium borohydride diammoniate. Chemistry of Materials 2010;22:6021–8.
[31] Guo YH, Xia GL, Zhu YH, Gao L, Yu XB. Hydrogen release from amminelithium borohydride, $LiBH_4{\bullet}NH_3$. Chemical Communications 2011;46:2599–601.
[32] Guo YH, Yu XB, Sun WW, Sun DL, Yang WN. The hydrogen-enriched Al–B–N system as an advanced solid hydrogen-storage candidate. Angewandte Chemie International Edition 2011;123:1119–23.
[33] Yuan F, Gu QF, Guo YH, Sun WW, Chen XW, Yu XB. Structure and hydrogen storage properties of the first rare-earth metal borohydride ammoniate: $Y(BH_4)_3{\bullet}4NH_3$. Journal of Materials Chemistry 2012;22:1061–8.
[34] Gu QF, Gao L, Guo YH, Tan YB, Tang ZW, Wallwork KS, et al. Structure and decomposition of zinc borohydride ammonia adduct: towards a pure hydrogen release. Energy & Environmental Science 2012;5:7590–600.
[35] Yuan F, Gu Q, Chen X, Tan Y, Guo Y, Yu X. Complex ammine titanium(III) borohydrides as advanced solid hydrogen-storage materials with favorable dehydrogenation properties. Chemistry of Materials 2012;24:3370–9.
[36] Guo YH, Sun WW, Guo ZP, Liu HK, Sun DL, Yu XB. Dehydrogenation promotion of $LiBH_4{\bullet}NH_3$ through heating in ammonia or mixing with metal hydrides. Journal of Physical Chemistry C 2010;114:12823–7.
[37] Guo YH, Jiang YX, Xia GL, Yu XB. Ammine aluminum borohydrides: an appealing system releasing over 12 wt.% pure H_2 under moderate temperature. Chemical Communications 2012;48:4408–10.
[38] Chen X, Yu X. Electronic structure and initial dehydrogenation mechanism of $M(BH_4)_2{\cdot}2NH_3$ (M = Mg, Ca, and Zn): a first-principles investigation. Journal of Physical Chemistry C 2012;116:11900–6.
[39] Guo YH, Wu H, Zhou W, Yu XB. Dehydrogenation tuning of ammine borohydrides using double-metal cations. Journal of the American Chemical Society 2011;133:4690–3.
[40] Tang ZW, Tan YB, Gu QF, Yu XB. A novel aided-cation strategy to advance the dehydrogenation of calcium borohydride monoammoniate. Journal of Materials Chemistry 2012;22:5312–8.
[41] Sun WW, Chen XW, Gu QF, Wallwork KS, Tan YB, Tang ZW, et al. A new ammine dual-cation (Li, Mg) borohydride: synthesis, structure, and dehydrogenation enhancement. Chemistry-A European Journal 2012;18:6825–34.

[42] Xia GL, Gu QF, Guo YH, Yu XB. Ammine bimetallic (Na, Zn) borohydride for advanced chemical hydrogen storage. Journal of Materials Chemistry 2012;22:7300–7.
[43] Soloveichik GL, Andrus M, Gao Y, Zhao JC, Kniajanski S. Magnesium borohydride as a hydrogen storage material: synthesis of unsolvated $Mg(BH_4)_2$. International Journal of Hydrogen Energy 2009;34:2144–52.
[44] Boultif A, Louër D. Powder pattern indexing with the dichotomy method. Journal of Applied Crystallography 2004;37:724–31.
[45] Kang X, Luo J, Zhang Q, Wang P. Combined formation and decomposition of dual-metal amidoborane $NaMg(NH_2BH_3)_3$ for high-performance hydrogen storage. Dalton Transactions 2011:3799–801.
[46] Custelcean R, Jackson JE. Dihydrogen bonding: structures, energetics, and dynamics. Chemical Reviews 2001;101:1963–80.
[47] Wolstenholme DJ, Titah JT, Che FN, Traboulsee KT, Flogeras J, McGrady GS. Homopolar dihydrogen bonding in alkali metal amidoboranes and its implications for hydrogen storage. Journal of the American Chemical Society 2011;133:16598–604.
[48] Wolstenholme DJ, Traboulsee KT, Hua Y, Calhoun LA, McGrady GS. Thermal desorption of hydrogen from ammonia borane: unexpected role of homopolar B-H•••H-B interactions. Chemical Communications 2012;48:2597–9.